Chinese Chemical Letters 34 (2023) 107770

Contents lists available at ScienceDirect

Chinese Chemical Letters

journal homepage: www.elsevier.com/locate/cclet

Tuning electron delocalization and surface area in COFs derived N, B co-doped carbon materials for efficient selective hydrogenation of nitroarenes

Hao Hu, Chunlei Song, Di Wang, Yinglong Tao, Shijian Zhou*, Yan Kong*

State Key Laboratory of Materials-Oriented Chemical Engineering, College of Chemical Engineering, Nanjing Tech University, Nanjing 210009, China

ARTICLE INFO

Article history:
Received 6 June 2022
Revised 1 August 2022
Accepted 21 August 2022
Available online 23 August 2022

Keywords:
N, B co-doped carbon materials
COFs carbonization
Molten salt assist
N species regulation
Hydrogenation of nitroarenes

ABSTRACT

Metal-free carbon catalysts with excellent conduction performance have drawn much research attention in reduction reactions. Herein, a N, B co-doped carbon catalyst with high pyrrolic N proportion (35.75%) and excellent surface area (1409 m^2/g) was successfully prepared *via* carbonizing covalent organic framework materials (COFs) containing N and B atoms assisted by $ZnCl_2$ molten salt. The presence of $ZnCl_2$ maintains the micropore structure of COFs to provide high specific surface areas and abundant lattice defects for carbon materials. In addition, electron-withdrawing B heteroatom further facilitates the formation of pyrrolic N at defect sites by modifying the electronic structure of carbon network. The tuning of surface areas and active N species in carbon catalysts successfully improve the selective hydrogenation of nitrobenzene to aniline. The optimized carbon material exhibits excellent nitrobenzene conversion (99.9%) and aniline selectivity (>99%) within 15 min, as well as excellent substrate suitability. This work provides a certain guiding for the design and application of metal-free catalysis.

As a kind of materials easily obtained from various precursors, porous carbon materials with easy preparation method and low preparation cost have attracted much attention in recent years [1,2]. But the inertness of π electrons provided by sp^2 hybridized carbon atoms and the limited surface areas obtained at high pyrolysis temperature make it is difficult for traditional carbon catalysts to exhibit outstanding in reactions that require electrons [3–5]. Therefore, heteroatomic doping and surface areas regulation are considered to be important strategies to achieve the construction of highly active carbon catalysts [6–8].

The similar atomic radius makes it is easy for N atoms to be introduced into the carbon skeleton by substituting lattice carbon to activate the π electrons in the carbon network [9–11]. Pyrrolic N with a pair of π-electrons, existing at the edges and defects of the carbon network, is considered as an ideal N-doping species to adjust the charge distribution on the surface of carbon skeleton, but the mixing of different nitrogen species (pyridinic N, pyrrolic N, graphitic N and oxidized N) is inevitable at high pyrolysis temperature [12,13]. Some reports indicate that the introduction of secondary heteroatom (*e.g.,* S, P and B) into the skeleton is considered as another effective strategy to modify its electronic structure, which can accelerates the formation of pyrrolic N at the defect and edge sites of carbon network [7,14]. Therefore, high surface area and abundant lattice defects are prerequisites for the formation of high pyrrolic N content.

2D covalent organic frameworks (COFs) are a class of fully predesignable polymers, which are achieved by topologically oriented polymer growth and geometric matching between monomers. The flexible design of building blocks and the orderliness of the topological structure make COFs possess high surface areas and become ideal precursors for heteroatom-doped carbons [1,15-17]. However, the direct carbonization of COFs usually leads to the collapse of pore structure due to mass loss and high surface energy [18].

Herein, a novel N, B co-doped porous carbon material with enhanced surface area and high pyrrolic N proportion was constructed by carbonizing covalent organic frameworks (COFs) containing N, B atoms assisted by $ZnCl_2$ (NBPC-Zn-X, X represents the pyrolysis temperature of COFs). The introduction of $ZnCl_2$ protect the intrinsic pore structure in precursors against shrinkage to support excellent surface areas and abundant lattice defects for carbons [19–21]. The flexible design of building blocks in COFs enables spatial separation of doped heteroatoms to avoid the poorly controlled entanglement under high temperature pyrolysis. In addition, it is observed that the presence of B heteroatom can effi-

* Corresponding authors.
E-mail addresses: zshijian@njtech.edu.cn (S. Zhou), kongy36@njtech.edu.cn (Y. Kong).

https://doi.org/10.1016/j.cclet.2022.107770
1001-8417/

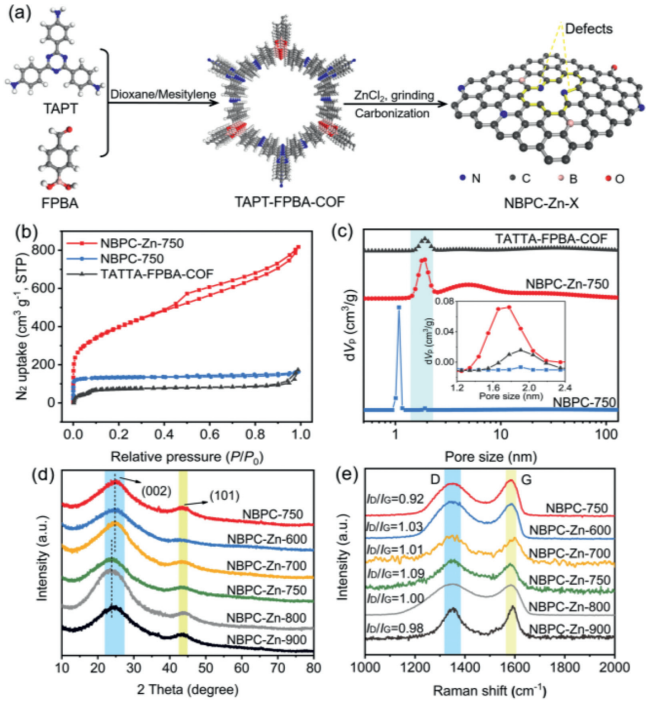

Fig. 1. (a) The preparation procedure of NBPC-Zn-X catalysts. (b) Nitrogen adsorption–desorption isotherms and (c) pore size distributions measured by non-local density functional theory (NL-DFT) method of samples. (d) PXRD patterns and (e) Raman spectra of NBPC-Zn-X and NBPC-750.

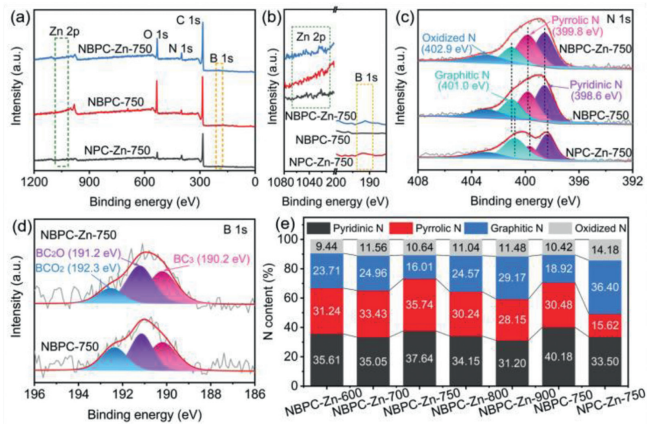

Fig. 2. (a) XPS survey spectra, (b) partial view of XPS spectrums and (c) high-resolution XPS N 1s spectrums of NBPC-Zn-750, NBPC-750 and NPC-Zn-750. (d) High-resolution XPS B 1s spectrums of NBPC-Zn-750 and NBPC-750. (e) The contents of specific N species in all fabricated materials.

ciently tailor the pyrrolic N proportion from 15.62% to 35.75%. The tuning surface areas and active N species in N, B co-doped carbon catalysts promotes the outstanding nitrobenzene reduction activity, high aniline selectivity, superior stability and broad substrate applicability. This also provides ideas for constructing efficient metal-free carbon catalysts.

The successful construction of COF precursor obtained by the condensation of 4-formylphenylboronic acid (FPBA) with 1,3,5-tris-(4-aminophenyl)triazine (TAPT) blocks was proved by power X-ray diffraction (PXRD, Fig. S2 in Supporting information) and Fourier transform infrared spectrometer (FTIR, Fig. S3 in Supporting information). The reasonable pyrolysis temperatures of TAPT-FPBA-COF should be maintained at 470–820 °C through thermogravimetric (TG) analysis (Fig. S4 in Supporting information). Subsequently, NBPC-Zn-X materials were synthesized *via* a "wet chemical" activation strategy (Fig. 1a). $ZnCl_2$ (m.p. is 283 °C; b.p. is 732 °C) can react as a solvent to maintain the microporous framework of TAPT-FPBA-COF against shrinkage and provide high surface areas and defects for carbon materials.

As exhibited in Fig. 1b, the Brunauer–Emmett–Teller (BET) surface area of TAPT-FPBA-COF is calculated to be 221 m^2/g, and this unsatisfactory surface area may be caused by the unreacted monomers in TAPT-FPBA-COF. After carbonization, the physisorption of NBPC-Zn-750 reveals the mixed type I and type IV isotherm (Fig. 1b), indicative of the co-existence of micropore and mesopore [15]. The BET surface area of NBPC-Zn-750 is calculated to be 1409 m^2/g, which is about 3.3 times that of NBPC-750 (434 m^2/g). Moreover, the pore diameter of NBPC-Zn-750 is maintained at about 1.8 nm estimated by NLDFT method (Fig. 1c), while this pore diameter almost disappears and a new pore size concentrated at about 1.1 nm appears in NBPC-750 (inset of Fig. 1c). These results imply that the molten $ZnCl_2$ filled in the TAPT-FPBA-COF can effectively support the large surface area and avoid the shrinkage of porous structure. However, with the increase of pyrolysis temperature, the gasification of $ZnCl_2$ will affect the meso– and macro-volumes of NBPC-Zn-X materials (Table S1 in Supporting information). For NPC-Zn-750 containing only N heteroatoms (Scheme S1, Figs. S7-S10 in Supporting information), the similar pore parameters to NBPC-Zn-750 (Table S1) indicates that the key to affecting the pore structure properties of carbons is $ZnCl_2$, which can render additional accessible active sites to improve catalytic activity [18,22].

The PXRD patterns of NBPC-Zn-X catalysts are displayed in Fig. 1d. The obvious diffraction peaks at 26.0° and 43.3° are indexed to the (002) and (101) facets of graphitic carbon, respectively [22]. It is worth noting that the (002) facet of catalyst shifts to a lower angle when pyrolysis temperature is higher than 750 °C, which may be caused by the effect of vaporized $ZnCl_2$ on the carbon multilayers structure [23]. In Raman spectra of samples. two peaks observed at 1325 cm^{-1} and 1595 cm^{-1} are attributed to the D- and G-bands (Fig. 1e), arising from the defective carbon and graphitic carbon, respectively [24]. The maximum value of I_D/I_G in NBPC-Zn-750 (1.09) reflects the highest defect density. This means that the vaporization of $ZnCl_2$ can cause lattice defects in the carbon skeleton, which are regarded as catalytically active and doping sites to adjust the charge delocalization in heteroatom-doped carbon network [1,22]. Moreover, the ratio of I_D/I_G in NPC-Zn-750 is estimated to be 1.07 (Fig. S11 in Supporting information), indicating the introduction of B heteroatom leads to more open defects.

The effect of the vaporization of $ZnCl_2$ on the NBPC-Zn-X samples is also reflected in their macroscopic morphologies. Compared to NPC-Zn-750 sample with smooth surface observed by field-emission scanning electron microscope (FESEM, Fig. S12 in Supporting information), gasified $ZnCl_2$ acts as a porogen to regulate the surface morphology of carbons (Fig. S13 in Supporting information).

The surface chemical composition of samples was investigated by X-ray photoelectron spectroscopy (XPS). As shown in Figs. 2a and b, there are no signals attributed to the Zn 2p orbitals detected in NBPC-Zn-750 and NPC-Zn-750, which can exclude the influence of metal ions on the catalytic activity. As displayed in Fig. 2c, there are four nitrogen species in NBPC-Zn-750 observed at 398.6 eV, 399.8 eV, 401.0 eV and 402.9 eV, corresponding to pyridinic N, pyrrolic N, graphitic N and oxidized N groups, respectively [25,26]. These peaks are also found in NPC-Zn-750 catalyst, but the signals of these specific N groups shift to lower binding energy compared with NBPC-Zn-750, suggesting the introduction of electron-deficient B can tune the electronic structure around N atoms to further improve charge delocalization in carbon networks. In B 1s spectrums (Fig. 2d), the peaks located at 190.2 eV, 191.2 eV

Table 1
XPS element contents in different catalysts.[a]

Entry	Catalysts	Temp. (°C)	Conv. (%)	Sel. (%)	TPF[d] (mol g^{-1} h^{-1})
1	NBPC-Zn-600	100	69.4	> 99	0.2776
2	NBPC-Zn-700	100	90.3	> 99	0.3612
3	NBPC-Zn-750	100	99.9	> 99	0.3996
4	NBPC-Zn-800	100	86.4	> 99	0.3456
5	NBPC-Zn-900	100	68.8	> 99	0.2752
6	NBPC-750	100	37.5	> 99	0.1500
7	NPC-Zn-750	100	73.9	> 99	0.2956
8[b]	NBPC-Zn-750	100	/	/	/
9[c]	None	100	1.4	> 99	0.0056

[a] Reaction conditions: 10 mg catalyst, 1 mmol nitrobenzene, 2 mL ethanol and 2 mL $N_2H_4{\cdot}H_2O$; reaction time: 15 min; the conversion and selectivity were determined by gas chromatograph-mass spectrometer (GC–MS).
[b] Without $N_2H_4{\cdot}H_2O$.
[c] Without catalyst.
[d] Turnover frequency (TOF) = (mole of the converted substrate)/(g catalyst × h (reaction time)).

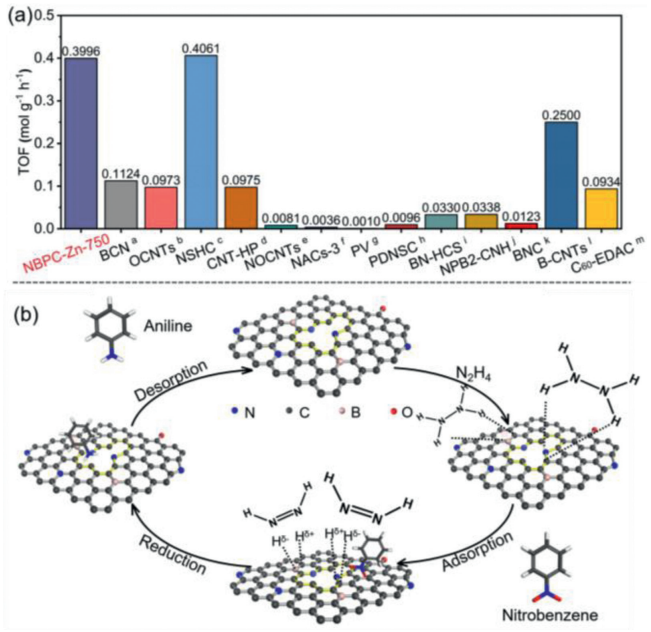

Fig. 3. (a) A comparison between the catalytic activity over NBPC-Zn-750 and other catalysts for nitrobenzene reduction (a: Ref. [33], b: Ref. [34], c: Ref. [35], d: Ref. [36], e: Ref. [37], f: Ref. [38], g: Ref. [29], h: Ref. [22], i: Ref. [39], j: Ref. [40], k: Ref. [31], l: Ref. [41], m: Ref. [42]). (b) Proposed mechanism for reduction of nitrobenzene by NBPC-Zn-X.

and 192.3 eV are attributed to the BC_3, BC_2O and BCO_2 species, respectively [27]. The similar N and B groups in NBPC-Zn-750 and NBPC-750 imply the chemical environment of doped heteroatoms is not affected by $ZnCl_2$. Moreover, there are no peaks of N–B bond found in NBPC-Zn-750 and NBPC-750 according to XPS analysis, which suggests that the specific positions of N and B atoms in the organic frameworks is favorable to avoid the adverse effects caused by the interaction between doped elements in carbon skeleton [5].

The content of specific N species in materials was tested by XPS and visualized in Fig. 2e (The N 1s spectrums of other samples are exhibited in Fig. S14 in Supporting information). NBPC-Zn-750 has the highest pyrrolic N content and the lowest graphitic N content in all catalysts, which are 35.75% and 16.01%, respectively. In contrast, NPC-Zn-750 exhibits the lowest pyrrolic N content (15.62%) and the highest graphitic N content (36.40%). Combined with Raman analysis, the gasification of $ZnCl_2$ and the introduction of B can open more lattice defects, and the electron-withdrawing B heteroatoms can modify the electronic structure of the carbon skeleton to induce the formation of active pyrrolic N at defect sites in NBPC-Zn-X [28]. The synergistic effect between electron-withdrawing B and electron-donating pyrrolic N can effectively regulate the π electron delocalization in the carbon network to improve the catalytic activity.

The catalytic activity of NBPC-Zn-X was evaluated by the reduction of nitrobenzene to aniline, and the reaction parameters are output in Table 1. The catalytic activity of catalysts shows a volcanic trend with the increase of annealing temperature (Fig. S15 in Supporting information), and the peak is appeared in the NBPC-Zn-750 with a remarkable TOF value of 0.3996 mol g^{-1} h^{-1} compared with others (Table 1, entries 1–5). The difference in performance over NBPC-Zn-X results from the high lattice defect density and pyrrolic N content. The combination of proper heteroatom doping and lattice defects has been proven to effectively improve the charge delocalization in skeleton and enhance the activity of selective hydrogenation of $-NO_2$ [29], but the content of graphitic N groups conjugated with sp^2 hybridized carbon atoms will increase with the improvement of the carbonization temperature. It is not conducive to breaking the electroneutrality of sp^2 carbon to create sites for the adsorption and activation of reactants [5]. As shown in entries 3, 6 and 7 of Table 1, the TOF value of NBPC-Zn-750 is about 2.7 and 1.4 times that of NBPC-750 (0.1500 mol g^{-1} h^{-1}) and NPC-Zn-750 (0.2956 mol g^{-1} h^{-1}), respectively. Therefore, the high catalytic activity of NBPC-Zn-750 can be attributed to the synergistic effects of the following factors: (i) The introduction of $ZnCl_2$ maintains the microporous properties of TATP-FPBA-COF, enabling NBPC-Zn-750 to have a high specific surface area for sufficient contact with nitrobenzene molecules; (ii) The vaporized $ZnCl_2$ can scour the carbon material and provide a large number of lattice defect sites when the pyrolysis temperature is slightly higher than the boiling point of $ZnCl_2$; (iii) The electron-deficient B can act as an electron acceptor to accommodate the π electrons of carbon materials due to its vacant p_z orbital, which promote the formation of pyrrolic N species with electron-donating properties at the defects or edges of the carbon framework. Finally, abundant active sites resulting from the $ZnCl_2$ and N, B co-doping decrease the Fermi energy level of carbonaceous material to regulate the adsorption of nitrobenzene and the activation of $N_2H_4{\cdot}H_2O$ [30–32].

Compared with other metal-free carbon-based catalysts, NBPC-Zn-750 shows excellent nitrobenzene reduction performance (Fig. 3a), which is close to the highest level compared with reported publications [22,29,31,33-42]. Meanwhile, NBPC-Zn-750 can still maintain a stable aniline yield after 6 cycles (Fig. S16 in Supporting information), and the morphology and structure of NBPC-Zn-750 have not obviously change after reaction (Figs. S17-S19 in Supporting information). The excellent catalytic reduction performance of NBPC-Zn-750 is also reflected in the suitability of the contact substrate. As listed in Table S2 (Supporting information), even if the steric hindrance and electronic properties of substrates are different, the high arylamines yield can still be achieved within 60 min [43].

As the key to investigate the reduction of $-NO_2$ to $-NH_2$ groups, the controlled experiments were tested to verify the source of active hydrogen species. As shown in Table S3 (Supporting information), the excellent aniline yield can be achieved in the presence of butylated hydroxytoluene (BHT) as a radical inhibitor, suggesting that ·H is not the key to the reduction reaction. Moreover, the formation of aniline is hardly discovered when $N_2H_4{\cdot}H_2O$ is replaced by H_2. Based on the above results and reported literature [22], a possible mechanism of nitrobenzene reduction over NBPC-Zn-X is illustrated in Fig. 3b. Specifically, $N_2H_4{\cdot}H_2O$ is adsorbed on the surface of catalysts and further activated at the N- and B-containing active sites. The hydrogen species generated by the cleavage of $N_2H_4{\cdot}H_2O$ would bond with N and B to form $N{-}H^{\delta+}$ and $B{-}H^{\delta-}$. In

addition, carbon atoms adjacent to N and B would also bond with hydrogen species to form C–$H^{\delta-}$ and C–$H^{\delta+}$, respectively. When nitroaromatic molecules are adsorbed on the surface of the carbon network, the oxygen atoms of nitro groups would extract the activated hydrogen atoms, resulting in the high selectivity of target products. Finally, arylamines are desorbed from the surface of the catalyst to complete the catalytic cycle.

In summary, N, B co-doped carbon porous materials (NBPC-Zn-X) were successfully prepared by carbonizing the TAPT-FPBA-COF precursor with the aid of $ZnCl_2$ as a medium. As the pyrolysis temperature increases, the different physical states of $ZnCl_2$ provide NBPC-Zn-X with high specific surface areas and abundant lattice defects. Meanwhile, the presence of electron-deficient B atoms further induces the formation of electron-rich pyrrolic N at defect sites of carbon network. Tuning surface area and pyrrolic N content in N, B co-doped materials can provide abundant active sites for the activation of $N_2H_4{\cdot}H_2O$ to achieve nitroarenes reduction. This work paves a way to design high-activity and non-metal-doped carbon catalysts.

Declaration of competing interest

The authors declare that they have no known competing financial interests or personal relationships that could have appeared to influence the work reported in this paper.

Acknowledgments

The authors acknowledge National Natural Science Foundation of China (Nos. 21776129 and 21706121), Natural Science Foundation of Jiangsu Province (No. BK20170995), Postgraduate Research & Practice Innovation Program of Jiangsu Province (No. KYCX21-1171) and the Project of Priority Academic Program Development of Jiangsu Higher Education Institutions (PAPD).

Supplementary materials

Supplementary material associated with this article can be found, in the online version, at doi:10.1016/j.cclet.2022.107770.

References

[1] Y.Q. Li, X.T. Xu, S.J. Hou, et al., Chem. Commun. 54 (2018) 14009–14012.
[2] C.H. Li, Z.Y. Yu, H.X. Liu, M. Xiong, Chem. Eng. J. 371 (2019) 433–442.
[3] Y.Q. Li, Z.B. Ding, X.L. Zhang, et al., J. Mater. Chem. A 7 (2019) 25305–25313.
[4] C. Yang, S. Maenosono, J.G. Duan, X.B. Zhang, ChemNanoMat 5 (2019) 957–963.
[5] Y. Zhao, L.J. Yang, S. Chen, et al., J. Am. Chem. Soc. 135 (2013) 1201–1204.
[6] Y.H. Xie, Y. Chen, L. Liu, et al., Adv. Mater. 29 (2017) 1702268.
[7] G.L. Chai, K.P. Qiu, M. Qiao, et al., Energy Environ. Sci. 10 (2017) 1186–1195.
[8] X.W. Lan, Y.M. Li, C. Du, et al., Chem. Eur. J. 25 (2019) 8560–8569.
[9] K.P. Gong, F. Du, Z.H. Xia, M. Durstock, L.M. Dai, Science 323 (2009) 760–764.
[10] R.L. Liu, D.Q. Wu, X.L. Feng, K. Mullen, Angew. Chem. Int. Ed. 49 (2010) 2565–2569.
[11] E.J. Yoo, J.J. Nakamura, H.S. Zhou, Energy Environ. Sci. 5 (2012) 6928–6932.
[12] Z.H. Sheng, L. Shao, J.J. Chen, et al., ACS Nano 5 (2011) 4350–4358.
[13] H.B. Wang, T. Maiyalagan, X. Wang, ACS Catal. 2 (2012) 781–794.
[14] J.T. Ren, C.Y. Wan, T.Y. Pei, X.W. Lv, Z.Y. Yuan, Appl. Catal. B: Environ. 266 (2020) 118633.
[15] C.C. Xu, Y. Su, D.J. Liu, X.Q. He, Phys. Chem. Chem. Phys. 17 (2015) 25440–25448.
[16] X.W. Hu, Y. Long, M.Y. Fan, et al., Appl. Catal. B: Environ. 244 (2019) 25–35.
[17] B. Ni, Y.Q. Li, T.Q. Chen, T. Lu, L.K. Pan, J. Colloid Interface Sci. 542 (2019) 213–221.
[18] Y.B. Huang, P. Pachfule, J.K. Sun, Q. Xu, J. Mater. Chem. A 4 (2016) 4273–4279.
[19] W.W. Lei, D. Portehault, R. Dimova, M. Antonietti, J. Am. Chem. Soc. 133 (2011) 7121–7127.
[20] N. Fechler, T.P. Fellinger, M. Antonietti, Adv. Mater. 25 (2013) 75–79.
[21] X.F. Liu, N. Fechler, M. Antonietti, Chem. Soc. Rev. 42 (2013) 8237–8265.
[22] X.W. Hu, X. Sun, Q. Song, et al., Green Chem. 22 (2020) 742–752.
[23] H. Hu, W.G. Kong, J. Wang, et al., Appl. Surf. Sci. 557 (2021) 149796.
[24] Z.H. Sun, Y. Liu, W.B. Ye, et al., Angew. Chem. Int. Ed. 60 (2021) 7180–7187.
[25] T. Sun, J. Wang, C.T. Qiu, et al., Adv. Sci. 5 (2018) 1800036.
[26] Z.Y. Lu, J. Wang, S.F. Huang, et al., Nano Energy 42 (2017) 334–340.
[27] W. Wang, P.D. Wang, Y.M. Kang, et al., Int. J. Hydrogen Energy 44 (2019) 4771–4779.
[28] H.N. He, D. Huang, Y.G. Tang, et al., Nano Energy 57 (2019) 728–736.
[29] R.J. Gao, L. Pan, J.H. Lu, et al., ChemCatChem 9 (2017) 4287–4294.
[30] L.J. Yang, S.J. Jiang, Y. Zhao, et al., Angew. Chem. Int. Ed. 50 (2011) 7132–7135.
[31] Y.R. Zhang, Y.Y. Zhai, M.Z. Chu, et al., Asian J. Org. Chem. 7 (2018) 1107–1112.
[32] D. Formenti, F. Ferretti, F.K. Scharnagl, M. Beller, Chem. Rev. 119 (2019) 2611–2680.
[33] G.M. Wang, P. Wang, X.F. Zhang, et al., Nanoscale 12 (2020) 7797–7803.
[34] Z.Z. Guo, N.Y. Zheng, L.Y. Zhang, et al., Phys. Chem. Chem. Phys. 22 (2020) 6524–6527.
[35] S.J. Liu, L.T. Cui, Z.Y. Peng, et al., Nanoscale 10 (2018) 21764–21771.
[36] S.C. Wu, G.D. Wen, R. Schlogl, D.S. Su, Phys. Chem. Chem. Phys. 17 (2015) 1567–1571.
[37] W. Xiong, Z.N. Wang, S.L. He, et al., Appl. Catal. B: Environ. 260 (2020) 118105.
[38] H.F. Wang, X.H. Li, Z.Y. Cui, L.J. Yang, S.J. Sun, React. Kinet. Mech. Catal. 130 (2020) 331–346.
[39] L.Y. Li, L. Li, C.Y. Cui, H.J. Fan, R.H. Wang, ChemSusChem 10 (2017) 4921–4926.
[40] X.H. Wu, L.B. Cui, P. Tang, et al., Chem. Commun. 52 (2016) 5391–5393.
[41] Y.M. Lin, S.C. Wu, W. Shi, et al., Chem. Commun. 51 (2015) 13086–13089.
[42] Y.B. Sun, C.Y. Cao, C. Liu, et al., Carbon 125 (2017) 139–145.
[43] S.C. Luo, Y. Long, K. Liang, et al., Green Chem. 23 (2021) 8545–8553.